Observations of five molecular species in absorption towards Sagittarius B2

Astron. Astrophys. 260, 381–390 (1992)

ASTRONOMY AND ASTROPHYSICS

Observations of five molecular species in absorption towards Sagittarius B2

J.S. Greaves[1], **Glenn J. White** [1,2], **M. Ohishi**[2], **T. Hasegawa**[2,3], **and K. Sunada**[2,3]

[1] Department of Physics, Queen Mary and Westfield College (University of London), Mile End Rd, London E1 4NS, United Kingdom
[2] Nobeyama Radio Observatory, Minamimaki, Minamisaku, Nagano 384-13, Japan
[3] Institute of Astronomy, Faculty of Science, University of Tokyo, Bunkyo-ku, Tokyo 113, Japan

Received September 13, accepted December 2, 1991

Abstract. Seven diffuse molecular clouds have been detected in absorption, using the Sgr B2 star-formation region as a source of background continuum emission. Transitions were observed at frequencies around 49, 85 and 98 GHz, from CS, $C^{34}S$, $H^{13}CN$, $H^{13}CO^+$, SiO and C_3H_2. Clouds detected in absorption include the "nuclear disk", the 3 kpc expanding arm, spiral arms in the Galactic Plane, and two unidentified regions. The nuclear disk line profile was found to be inconsistent with homogeneous disk or bar models, instead suggesting irregular perturbations of the gas within a few hundred pc of the Galactic Centre.

Absorption in CS was detected in two different rotational transitions, leading to reliable estimates of the physical parameters of the clouds. In particular, excitation temperatures could be estimated, instead of assumed values being used, as was the case in previous studies. Results from an LTE analysis and from LVG modelling show that the absorption lines are mostly optically thin, with molecular column densities $\sim 10^{12-14}$ cm^{-2} per cloud. Excitation temperatures as high as 5 K were found, inconsistent with heating by the 2.7 K cosmic background radiation alone. Cloud densities were estimated at $n_{H_2} \sim 10^4$ cm^{-3}, or less if the gas is highly subthermalised.

Key words: Galaxy (the): structure of – interstellar medium: abundances – interstellar medium: clouds: Sgr B2 – interstellar medium: molecules

1. Introduction

Few studies have been made of diffuse molecular clouds (densities $n_{H_2} \sim 10^{3-4}$ cm^{-3}). This is because excitation temperatures may be as low as 2.7 K (in equilibrium with the cosmic background radiation); hence, few molecules are excited out of the $J=0$ rotational level, and emission lines are, therefore, very weak. However, when these clouds lie in front of a bright, millimetre, continuum source, *absorption* lines may be observed, from a range of molecular species. Molecules including CS, CN, CCH, HCN, HNC, HCO^+, H_2CO and C_3H_2 have been detected in absorption, along lines of sight towards H II regions in Sgr A, W 49, W 51 and DR 21, and the SNR Cas A (Kogut et al. 1989; Nyman 1983, 1984; Nyman & Millar 1989; Cox et al. 1988). These observations are beginning to reveal the chemistry and structure of diffuse clouds. Of particular interest are the features around the Galactic Centre, and in spiral arms. In the latter, the diffuse clouds may be the precursors of denser cores in which high-mass stars form; hence, the absorption line observations are important for evidence of the initial composition. The relative molecular and atomic abundances affect processes such as cloud heating and cooling during the collapse stage of star formation (Hollenbach 1988).

The high-mass star-forming core Sagittarius B2 has been used as a background source for the observations presented in this paper. Sgr B2 is located ~ 100 pc from the Galactic Centre (Lis & Goldsmith 1990). The continuum radiation at millimetre wavelengths arises from the H II regions surrounding two young stars, which are embedded in dense molecular gas. Located in front of the cloud cores is a cooler, more diffuse cloud envelope, with kinetic temperature T_{kin} only ~ 10–20 K (Lis & Goldsmith 1990). Finally, in the foreground along the line of sight, there are seven cool diffuse clouds. These include gas in spiral arms; expanding features at galactocentric distances of 3–4 kpc; the "nuclear disk" (a body of diffuse gas extending out to ~ 1 kpc from the Galactic Centre, Sanders et al. 1984); and also unidentified clouds.

The continuum spectrum of Sgr B2, against which the diffuse clouds are seen in absorption, consists of free–free emission at wavelengths $\gtrsim 3$ mm and thermal blackbody emission (from dust) at shorter wavelengths (Gordon et al. 1986; Goldsmith et al. 1987, 1990). The measured flux from the continuum source depends on the beamsize (due to the presence of extended diffuse emission) as well as on factors such as telescope efficiency and coupling. For the main condensations, peak antenna temperatures (on differently calibrated scales) have been reported in the range 0.5–10 K at millimetre wavelengths. Molecular line absorption features against this strong continuum have been reported by several authors [e.g. HCO^+ and HCN observations by Linke et al. (1981), C_3H_2 by Matthews & Irvine (1985) and H_2CO by Downes et al. (1980)].

In the present observations, absorption lines from 5 species (plus a CS isotopomer) have been detected towards the Sgr B2 "M" and "N" cores. Additionally, lower S/N detections have been obtained at surrounding positions (Table 1). These observa-

Send offprint requests to: J.S. Greaves

Table 1. Positions observed. The reference position used was RA(1950) = $17^h44^m10.6^s$, Dec(1950) = $-28°22'05''$. The positions listed are those observed at NRO except where stated otherwise

Position	Offset (arcsec)	
	δRA	δDec
Sgr B2 "M" (JCMT)	− 3	+ 2
Sgr B2 "M"	− 5	0
Sgr B2 "N"	− 15	+ 45
1	+ 15	0
2	− 25	0
3	− 5	+ 20
4	− 5	− 20
5	+ 5	+ 45
6	− 35	+ 45
7	− 15	+ 65
8	− 15	+ 25

tions have been used to calculate physical parameters for the diffuse clouds (results are presented in Sect. 3), and the velocities at which absorption was detected have enabled the features to be identified (discussed in Sect. 4).

Table 2. Transitions observed. The listed ν_0 are the rest frequencies of the transitions, and the E_l values are the energies of the lower levels of the transitions, relative to the $J = 0$ level. The three $H^{13}CN$ hyperfine components were not resolved; velocities were derived from the central component

Species	Transition	ν_0 (GHz)	E_l/k (K)
$C^{34}S$	$J = 1–0$	48.2070	0.0
CS	$J = 1–0$	48.9910	0.0
C_3H_2	$J_{K-1,K_1} = 2_{1,2}–1_{0,1}$	85.3389	1.7
$H^{13}CN$	$J = 1–0$ $F = 1–1$	86.3388	0.0
$H^{13}CN$	$J = 1–0$ $F = 2–1$	86.3402	0.0
$H^{13}CN$	$J = 1–0$ $F = 0–1$	86.3423	0.0
$H^{13}CO^+$	$J = 1–0$	86.7543	0.0
SiO	$J = 2–1$	86.8470	2.1
CS	$J = 2–1$	97.9810	2.4
CO	$J = 2–1$	230.5380	5.5
^{13}CO	$J = 3–2$	330.5880	15.9
$C^{34}S$	$J = 7–6$	337.3966	48.6
CS	$J = 7–6$	342.8829	49.4
CO	$J = 3–2$	345.7960	16.6
$H^{13}CO^+$	$J = 4–3$	346.9985	25.0
HCN	$J = 4–3$	354.5055	25.5
HCO^+	$J = 4–3$	356.7342	25.7

2. Observations

Observations were obtained during November and December, 1987, using the 45 m telescope at the Nobeyama Radio Observatory (NRO), Japan, and additional observations were made during February, July and September, 1988 at the James Clark Maxwell Telescope (JCMT), located on Mauna Kea, Hawaii.

For the NRO observations, the receiver system used cooled Schottky-diode mixers (in the 49, 85 and 98 GHz regions) and an SIS mixer (in the 42 GHz region). The mixers were operated in single-sideband mode with a polarisation beam-splitter and an acousto-optical spectrometer (AOS). The 8 AOS banks, each of 2048 channels, gave a total passband of 2 GHz (250 MHz per bank). The frequency resolution was 0.25 MHz (0.8–1.8 km s^{-1} at 98–42 GHz). Single sideband system noise temperatures on the sky were ≈500 K for the Schottky-diode mixer and ≈300 K for the SIS mixer. The beamwidths ranged from ≈40″ at 42 GHz to ≈20″ at 98 GHz, with relative pointing errors of ≲ 8″ throughout. The spectra are presented on a main-beam antenna temperature scale, T_{mb}, with main-beam efficiencies η_{mb} (known to within ∼ ± 10%) of 0.65 at 42 GHz, 0.75 at 49 GHz, 0.52 at 85 GHz and 0.46 at 98 GHz. Baselines were determined by position switching, with an off position at δRA = −30′. (Inspection of the maps by Bally et al. (1987) showed that this off position is free of emission, with antenna temperatures <0.1 K for CS $J = 2 – 1$.) The raw data for the on and off positions were inspected, in regions of the spectra which were free of lines, in order to obtain a first-order estimate of the continuum temperature.

The absorption lines were observed in the course of a biased spectral survey of the two cores (White et al. in preparation). The positions Sgr B2 "M" and "N" were observed in the frequency ranges 42.5–43.0, 47.5–48.5 and 48.55–49.05 GHz. These two positions, plus the 8 surrounding points, were then observed at 85.0–85.5, 85.9–86.9 and 97.55–98.05 GHz. Integration times on the source were ∼30 min at Sgr B2 "M" and Sgr B2 "N", and ∼10 min at the other positions.

Additional observations were made with the JCMT at higher frequencies, using shorter integration times (∼150 s on source). No absorption lines from the diffuse foreground clouds were detected. The observed transitions are listed in Table 2.

For the JCMT observations, cooled Schottky-diode receivers were used in double-sideband mode, with a 500 MHz AOS passband comprising 512 channels with spectral resolution ≈1 MHz (corresponding to 1.3 km s^{-1} at 230 GHz and 0.9 km s^{-1} at 345 GHz). The single sideband system noise temperature on the sky was ∼4000 K. Observations were again made in position-switching mode, with a beamwidth of 21″ at 230 GHz and 14″ at 345 GHz. Pointing errors were ≲ 10″. The spectra are again presented on a T_{mb} antenna temperature scale, with η_{mb} values of 0.5 for CS, $C^{34}S$ $J = 7–6$, HCO^+, $H^{13}CO^+$ $J = 4–3$ (February, 1988), and 0.55 for CO, ^{13}CO $J = 3–2$, HCN $J = 4–3$ and 0.6 for CO $J = 2–1$ (July and September, 1988). The errors in the η_{mb} values are ∼10%, but may be somewhat larger for the earliest observing period, when considerable improvements were made to the telescope over only a few months. At the times of the observations, the surface accuracy of the JCMT was estimated at 45 μm rms.

3. Results

Of the 50 molecular transitions detected in the NRO spectral survey of Sgr B2 (White et al., in preparation; Greaves 1990), 11 showed absorption. These profiles can be divided into two types: absorption against the continuum alone (7 transitions), and absorption combined with molecular emission from the Sgr B2 core. Examples of the spectra are presented in Fig. 1, and the

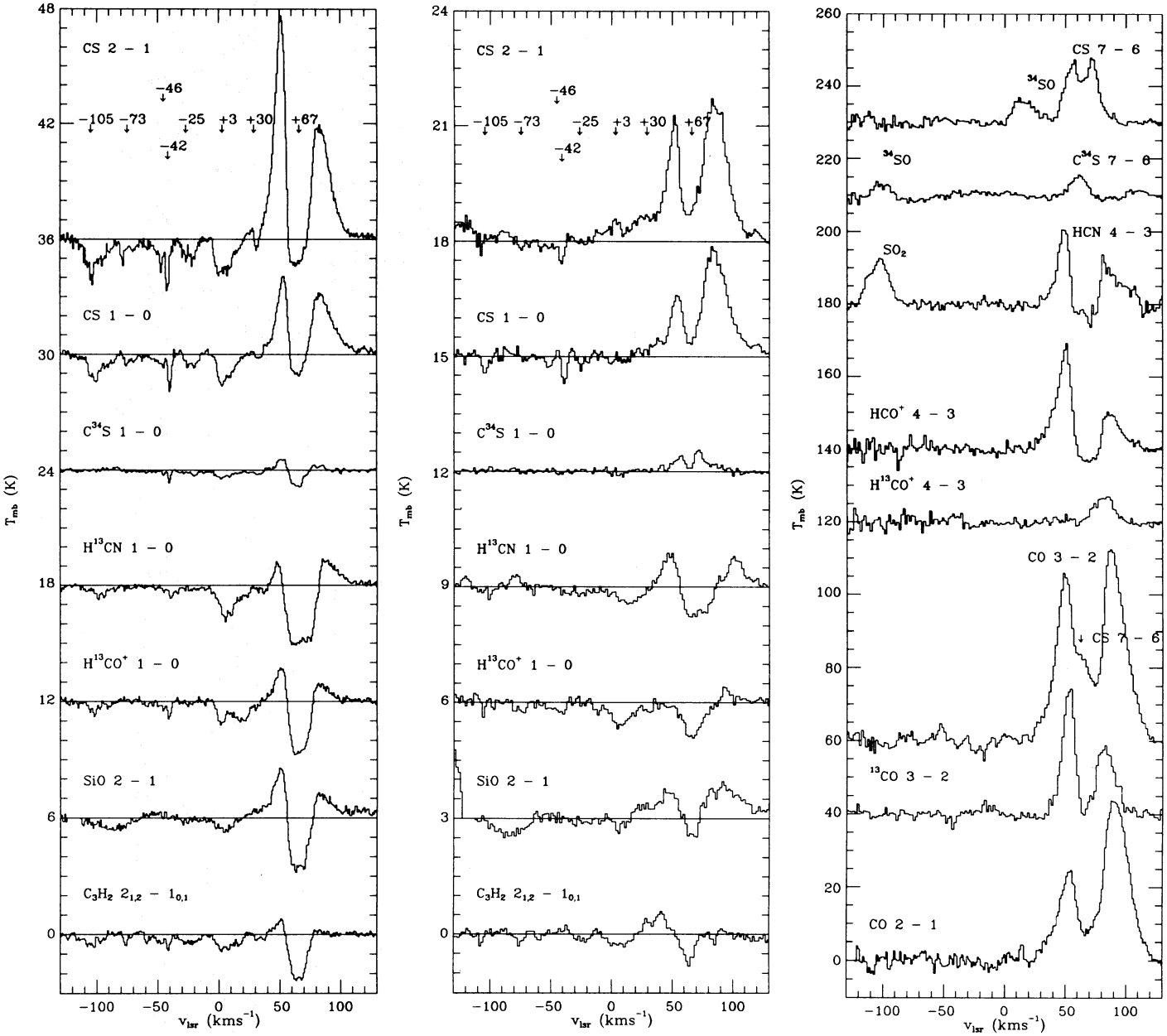

Fig. 1a–c. Examples of the spectra. **a** NRO spectra towards Sgr B2 "M", showing absorption lines from foreground clouds. Relative T_{mb} offsets are used for clarity. The characteristic velocities of the individual clouds are indicated with arrows above the CS $J=2$–1 spectrum. **b** NRO spectra towards Sgr B2 "N", otherwise as for **a**. The feature at $v_{lsr} \approx -130$ km s^{-1} in the SiO spectrum is a methanol line from the Sgr B2 "N" core. **c** JCMT spectra. Absorption is seen only at $v_{lsr} = +67$ km s^{-1}, from the cloud physically associated with the Sgr B2 cores. The velocity scale for $H^{13}CO^+$ $J=4$–3 is in error by $\approx +20$ km s^{-1}. The CS $J=7$–6 line superimposed on CO $J=3$–2 is from the other sideband

measured line characteristics are given in Table 3. No absorption lines from the foreground clouds were detected in the JCMT spectra. More recently, HCN $J=4$–3 has been seen in absorption against the Sgr B2 continuum (Lis & Goldsmith 1991), at $v_{lsr} \approx 0$ km s^{-1}. Since the line strength was only -0.5 K (T_A^*), it is not surprising that this line was not detected in the JCMT spectrum presented here [T_R^*(rms) ≈ 0.5 K].

The velocities of the absorption minima fall into distinct groups around $v_{lsr} = +67$, $+30$, $+3$, -25, -42, -46, -73 and -105 km s^{-1}. These velocities are the radial velocities of molecular clouds along the line of sight towards Sgr B2. Identifications of the clouds will be discussed in Sect. 4.

3.1. *LTE data analysis*

A local thermodynamic equilibrium (LTE) approach was initially used to analyse the spectra, since there is currently little evidence for temperature gradients or clumping in these clouds, which would invalidate the LTE assumptions. Since the relevant equa-

Table 3. Characteristics of absorption lines – NRO observations. T_{mb} and v_{lsr} are the main-beam brightness temperature and the local standard of rest velocity values for the line minimum, and Δv is the full width at the half minimum point. T_{mb} is in K and the velocities are in km s^{-1}. An asterisk before the FWHM value denotes a blend of features within a cloud. A blank entry indicates no detection or that the transition was not observed. Errors on v_{lsr} and Δv are ~ 1 km s^{-1} for narrow features, increasing to ~ 10 km s^{-1} for weak broad lines. Rms errors on T_{mb} are ≈ 0.03–0.5 K, and can be estimated from the spectra (Fig. 1)

Position	CS $J = 1$–0			CS $J = 2$–1			$C^{34}S$ $J = 1$–0			SiO $J = 2$–1		
	T_{mb}	v_{lsr}	Δv	T_{mb}	v_{lsr}	Δv	T_{mb}	v_{lsr}	Δv	T_{mb}	v_{lsr}	Δv
M	− 0.2	33	3	− 0.4	30	3	0.1	34	8			
M	− 1.5	3	14	− 2.0	0	13	− 0.3	− 1	8	− 0.7	5	4
N										− 0.4	5	6
M	− 0.6	− 21	*11	− 1.0	− 24	10	− 0.1	− 21	5			
M	− 0.6	− 26	*11									
1										− 0.9	− 27	20
M	− 2.0	− 41	2	− 2.5	− 43	3	− 0.7	− 40	2			
M	− 0.6	− 45	2	− 1.4	− 48	3	− 0.4	− 45	3			
N	− 0.7	− 40	5	− 0.6	− 41	5						
M	− 0.5	− 76	9	− 1.0	− 78	14				− 0.6	− 87	6
N										− 0.5	− 84	25
M	− 1.3	− 102	11	− 2.1	− 104	9						
N	− 0.5	− 105	5									
1				− 1.2	− 105	6						

Position	$H^{13}CN$ $J = 1$–0			$H^{13}CO^+$ $J = 1$–0			C_3H_2 $2_{1,2}$–$1_{0,1}$		
	T_{mb}	v_{lsr}	Δv	T_{mb}	v_{lsr}	Δv	T_{mb}	v_{lsr}	Δv
M	− 0.3	35	6	− 1.0	19	14	− 0.3	30	4
M							− 0.3	38	3
N	− 0.4	13	22						
M	− 1.6	5	10	− 1.2	2	7	− 0.8	8	*14
M							− 0.8	2	*14
N				− 0.6	5	17	− 0.3	7	17
N				− 0.3	− 11	6			
1				− 1.1	− 10	27			
7	− 0.8	11	22						
M							− 0.5	− 24	17
N							− 0.3	− 24	11
1	− 0.8	− 27	25						
2	− 0.3	− 24	22						
M	− 0.7	− 40	6	− 0.8	− 41	6	− 0.7	− 42	5
M							− 0.5	− 47	7
N				− 0.3	− 39	11			
M							− 0.5	− 59	3
M							− 0.6	− 77	2
N				− 0.3	− 71	8	− 0.3	− 75	3
1				− 0.8	− 71	14			
M	− 0.6	− 103	11	− 0.7	− 102	10	− 0.6	− 102	11
N							− 0.3	− 109	3

tions differ from those commonly used to analyse emission line data, a brief summary is given in Appendix A.

In order to estimate the limiting values of optical depth and excitation temperature, LTE calculations were initially made using the simplest possible assumptions. These are that either $\tau \gg 1$ (from which the upper limit on T_{ex} can be found), or that $T_{ex} = 2.7$ K, in equilibrium with the cosmic background radiation (giving lower limits on τ). For the first case, $T_{ex} \lesssim 7$ K is found, and for the second, $\tau \gtrsim 0.02$–0.6, depending on the line strength. Results from two more complex approaches to the radiative

transfer problem are discussed below, and for these the optical depth and excitation temperatures lie between the above limits, as expected.

The optical depth and column density estimates are significantly affected by the excitation temperature used. Previous authors (e.g. Nyman & Millar 1989; Nyman 1984, 1983) have generally assumed $T_{ex}=2.7$ K, but a more accurate value can be calculated from the observations presented here. T_{ex} values were estimated using the CS $J=1$–0 and 2–1 transitions, in Eq. (A6). For the clouds at $v_{lsr}=+3$ and -105 km s^{-1}, the excitation temperature was found to be ≈ 3 K, and for the clouds at $+30$, -25, -44 (double feature) and -73 km s^{-1}, T_{ex} was 4–5 K. The errors are ~ 1 K (from the errors in the antenna temperature ratios), but several of the values are definitely inconsistent with equilibrium with the cosmic background radiation.

T_{ex} could not be calculated for other species, and the modelling results presented in a later section suggest that T_{ex} varies between transitions. Also, for lines which absorb almost all the continuum emission, T_{ex} is constrained to be close to 2.7 K by Eq. (A2). Hence, it may not be valid to use the CS excitation temperatures to calculate the column densities and optical depths for all the species. Instead the lower and upper values found for T_{ex} (2.7 and 5 K) have been used to estimate the corresponding τ and N (Table 4). The small difference of 2.3 K between the two excitation temperatures can have a large effect on the optical depth estimate, with τ greater by factors up to 4 for $T_{ex}=5$ K, compared to $T_{ex}=2.7$ K.

The lines were found to be mostly optically thin, with τ as high as 2 only in a few cases with $T_{ex}=5$ K. The column densities found were $N\sim 10^{12-14}$ cm^{-2}, with an upper limit $\sim 10^{12}$ cm^{-2} where no detection was obtained. (The exact value of the upper limit depends on the species observed and the noise level of a particular scan.)

To search for variations in chemistry between the different clouds, the ratio N(species)/N(CS) was evaluated. [The abundance of CS is known to vary when shocks are present (e.g. Hartquist et al. 1980), but this should not be the case for diffuse clouds with no known embedded sources.] The column density ratios mostly varied by small factors (≤ 3) from cloud to cloud, and these can be explained by the excitation differences estimated above. However, the profiles observed for C_3H_2 and SiO are different from those of the other species, especially at -40 to -90 km s^{-1}, indicating variations in abundances, excitation or location.

The isotopic ratio [^{32}S/^{34}S] has been estimated from the CS and C^{34}S column densities. The values found were 6–9. 7–8, and 8–15, for clouds at $v_{lsr}=+3$, -25 and -44 km s^{-1}. The ranges quoted include the variations between $T_{ex}=2.7$ and 5 K, and also from the omission of inclusion of an escape probability factor $(1-e^{-\tau})/\tau$. The value of τ used was that for the line minimum, and the optical depth away from the central velocity will be less; hence, the upper value for the isotopic ratio is likely to be overestimated. The largest source of error (not included above) is the baseline uncertainty on the C^{34}S spectra, which could change the ratios by $\sim 30\%$. The assumption that [32S/^{34}S] = [C^{32}S/C^{34}S] should be valid provided that T_{ex} is similar for the two species, there is no isotopic fractionation, and that the molecules are distributed over the same length of line-of-sight gas.

The isotopic ratio [^{32}S:^{34}S] is, therefore, $\sim$6–15, small compared to the average in dark clouds of 20 (with variations $\approx \pm 5$) (Wannier 1980), and the terrestrial value of 23. The diffuse clouds, therefore, appear to be overabundant in ^{34}S, an element which may be ejected from high-mass stars, as are other heavy rare isotopes (Tosi 1982). Since the diffuse clouds are located in spiral arms and near the Galactic Centre (Sect. 4.1), regions where high-mass star-formation occurs, this may explain the low [^{32}S:^{34}S] ratio. Since sulphur has not yet been included in Galactic chemical evolution models, this result is inconclusive.

In all the LTE calculations, it has been assumed that T_{mb}(c) is constant over the 42–98 GHz region, since the continuum strength was only measured at 42 GHz. At frequencies $\lesssim 100$ GHz, the continuum emission from Sgr B2 has a free–free spectrum (Goldsmith et al. 1987), which is nearly flat, with flux $S_\nu \propto \nu^{-0.1}$. Since $T_{mb}(c) \propto S_\nu/(\nu^2 \mathrm{FWHM}^2)$ for a compact source, and the beam has FWHM $\propto \nu^{-1}$, it follows that $T_{mb}(c) \propto S_\nu$ and can, therefore, be considered to be approximately constant for the 42–98 GHz NRO observations. (This ignores the fact that more of the extended diffuse emission component is present in the larger beam at 42 GHz than at 98 GHz. Akabane et al. (1988), using the NRO 45 m telescope, find that at 43 GHz the flux density of the extended component is only $\sim 10\%$ of that of the Sgr B2 "M" compact continuum source.)

The continuum strengths were estimated to be $T_{mb}(c)=4.5 \pm 1.2$ K at "M" and 2.2 ± 1.1 K at "N". The errors are rms, and result from atmospheric fluctuations between scans. Calibration from the 43 GHz continuum map of Akabane et al. (1988), also made with the NRO 45 m telescope, was used to estimate T_{mb}(c) at the other positions.

It should be noted that these T_{mb}(c) values are lower than the 10.5 and 6.7 K found for "M" and "N", respectively, in the Akabane et al. (1988) 43 GHz continuum map. These differences are likely to be due to relative pointing offsets, since the Akabane et al. data show that the reduction in observed continuum strengths can be explained by 25″–30″ position offsets, and the measured (relative) pointing errors were $\lesssim 15''$ and $\lesssim 8''$ in the continuum and line observations, respectively. The T_{mb}(c) values from the current data were used for the calculations, since the line and continuum values are consistent. For example, the continuum appears almost wholly absorbed in H^{13}CN $J=1$–0 at "M", $v_{lsr}=60$ km s^{-1}, consistent with $T_{mb}(l)=-3.1$ K, and $T_{mb}(c)=4.5 \pm 1.2$ K.

3.2. *LVG modelling*

In order to estimate the importance of radiative transfer effects, a large-scale velocity gradient (LVG) model has also been used to analyse the data. The main advantages of this model over the LTE calculations are that T_{ex} is calculated in the modelling and that the output consists of density and abundance solutions, which cannot be found by LTE methods.

The model used consists of a continuum source, the 2.7 K cosmic background radiation, and a foreground molecular cloud. This cloud is assumed to have uniform temperature and density, and its kinematics are dominated by large-scale motions (turbulence is neglected). The velocity field used assumed $v \propto r$, where r is the distance to the centre of the cloud; thus, all points along a line of sight have different velocities towards the observer. Radiation emitted at one position can, therefore, not be absorbed elsewhere in the cloud, which greatly simplifies the calculation of the level populations and line strengths.

Table 4. Results of LTE analysis. The values shown are the line-minimum optical depths (τ) and the total column densities (N). For $T_{ex} = 2.7$ K the results for the "M" and "N" positions are averaged where both were detected. For $T_{ex} = 5$ K results were only found for "M". Column densities for CS $J = 1$–0 and $J = 2$–1 have also been averaged. Escape probability corrections to N have been omitted. A hyphen (-) indicates that there was no detection and an asterisk (*) that the observed line strengths were inconsistent with $T_{ex} = 5$ K

Table 4a. Results for $T_{ex} = 2.7$ K

v_{lsr} (km s^{-1})		CS	$C^{34}S$ $J = 1$–0	SiO $J = 2$–1	$H^{13}CN$ $J = 1$–0	$H^{13}CO^+$ $J = 1$–0	C_3H_2 $2_{1,2}$–$1_{0,1}$
+ 30	τ	0.05 ($J = 1$–0) 0.1 ($J = 2$–1)	0.05	—	0.2	0.2	0.1
	N (10^{13} cm^{-2})	0.2	0.1	—	0.1	0.5[a]	0.3
+ 3	τ	0.3 ($J = 1$–0) 0.5 ($J = 2$–1)	0.05	0.2	0.4	0.3	0.2
	N (10^{13} cm^{-2})	4.2	0.6	0.5	0.9	0.5[a]	2.0
− 25	τ	0.1 ($J = 1$–0) 0.3 ($J = 2$–1)	0.02	—	—	—	0.1
	N (10^{13} cm^{-2})	1.6	0.2	—	—	0.5[a]	1.1
− 44[b]	τ	0.5 ($J = 1$–0) 0.6 ($J = 2$–1)	0.2	—	0.2	0.2	0.2
	N (10^{13} cm^{-2})	2.8	0.2	—	0.2	0.1	1.1
− 73	τ	0.1 ($J = 1$–0) 0.3 ($J = 2$–1)	—	0.2	—	0.1	0.2
	N (10^{13} cm^{-2})	1.3	—	1.3[a]	—	0.1	0.6
− 105	τ	0.3 ($J = 1$–0) 0.6 ($J = 2$–1)	—	—	0.1	0.2	0.2
	N (10^{13} cm^{-2})	4.4	—	1.3[a]	0.2	0.1	1.0

Table 4b. Results for $T_{ex} = 5$ K

v_{lsr} (km s^{-1})		CS	$C^{34}S$ $J = 1$–0	SiO $J = 2$–1	$H^{13}CN$ $J = 1$–0	$H^{13}CO^+$ $J = 1$–0	C_3H_2 $2_{1,2}$–$1_{0,1}$
+ 30	τ	0.1 ($J = 1$–0) 0.2 ($J = 2$–1)	0.05	—	0.1	0.5	0.1
	N (10^{13} cm^{-2})	0.3	0.2	—	0.2	1.0[a]	1.1
+ 3	τ	1.0 ($J = 1$–0) 1.8 ($J = 2$–1)	0.1	0.3	1.1	0.7	0.4
	N (10^{13} cm^{-2})	9.6	1.9	1.1	2.7	1.0[a]	7.4
− 25	τ	0.3 ($J = 1$–0) 0.5 ($J = 2$–1)	0.05	—	—	—	0.2
	N (10^{13} cm^{-2})	3.4	0.5	—	—	—	3.7
− 44[b]	τ	1.8 ($J = 1$–0) * ($J = 2$–1)	0.3	—	0.3	0.4	0.3
	N (10^{13} cm^{-2})	*	0.7	—	0.5	0.2	4.1
− 73	τ	0.2 ($J = 1$–0) 0.5 ($J = 2$–1)	—	0.3	—	—	0.3
	N (10^{13} cm^{-2})	2.8	—	1.8[a]	—	—	1.1
− 105	τ	0.8 ($J = 1$–0) 2.1 ($J = 2$–1)	—	—	0.3	0.3	0.3
	N (10^{13} cm^{-2})	9.8	—	1.8[a]	0.8	0.2	4.6

[a] Combined N for more than one velocity, since the spectra are blended
[b] Combined absorption $v_{lsr} = -42$ and -46 km s^{-1}; the optical depths given are for -42 km s^{-1}

Model runs have been done for cloud kinetic temperatures T_{kin} of 10–50 K, using standard collisional excitation rates. Results were found for absorption lines seen towards Sgr B2 "M" only, as there was insufficient data to constrain the solutions towards the other positions. Initially, solutions were sought for density (n_{H_2}) and molecular abundance relative to H_2 divided by velocity gradient [$X/(dv/dr)$], that reproduce the observed T_{mb}(l) for CS $J=1$–0 and 2–1 (Fig. 2). The hydrogen densities found were then used in conjunction with T_{mb}(l) for other transitions, to estimate $X/(dv/dr)$ for the other species. The results of the LVG modelling are given in Table 5. The values quoted assume $T_{kin}=10$ K (collisional rates were not generally available for lower temperatures, and cannot be reliably extrapolated), and the ranges given take into account the errors on T_{mb}(l) and consequent error in the antenna temperature ratio of CS $J=1$–0 to CS $J=2$–1. An additional source of error is the uncertainty in T_{mb}(c), which results in smallar systematic errors [$\lesssim 0.2$ in $\log n_{H_2}$ and $\log X/(dv/dr)$].

The optical depths found from the LVG model are mostly less than 1, and in good agreement with the LTE calculations for $T_{ex}=2.7$ K (differing on an average by $\Delta\tau \approx 0.1$). This suggests that the simplifications and assumptions in the model do not greatly affect the results. (If turbulence is present, the chance of an emitted photon being absorbed elsewhere in the cloud remains small for $\tau < 1$; hence, radiative coupling of different areas of the cloud is negligible.) The excitation temperatures from the LVG analysis (2.7–4.1 K) are also consistent with the LTE results.

The average cloud density was found to be $n_{H_2} \approx 10^4$ cm^{-3}, somewhat higher than the 10^3 cm^{-3} often quoted for diffuse clouds (e.g. Irvine et al. 1987). The values of $X/(dv/dr)$ vary substantially from cloud to cloud, by as much as an order of magnitude. This could be due to either chemical differences, or variations in the velocity gradient. Since the ratio of $[X(CS)/(dv/dr)]/[X(C_3H_2)/(dv/dr)]$ varies by much less (a factor of only 2.5 over 6 clouds), it appears that the clouds are chemically similar (as also found by LTE analysis), but have different velocity gradients.

Assuming [^{12}C:^{13}C] values ~50–90, for HCN and HCO$^+$ the $X/(dv/dr)$ values are ~(1–2) 10^{-9} and ~(5–9) 10^{-10} km^{-1} s pc, respectively. For dense clouds, the abundances (X) of HCN and HCO$^+$ are slightly greater (e.g. 5 10^{-9} and 2 10^{-9}, respectively, in the Orion molecular ridge, Blake et al. 1987). Hence the LVG results suggest similar abundances in both types of cloud (for velocity gradients ~1 km s^{-1} pc^{-1} in the diffuse gas, as found by Greaves & Williams, in preparation).

Using the average value $X(C_3H_2)/(dv/dr) = 2\ 10^{-11}$ km^{-1} s pc, and assuming $dv/dr \sim 1$ km s^{-1} pc^{-1}, $X(C_3H_2)$ is ~$2\ 10^{-11}$. This is considerably smaller than the $X \sim 10^{-9}$–10^{-8} found by Cox et al. (1988) for diffuse clouds seen in absorption towards 5 galactic and extragalactic continuum sources. This difference arises because the Cox et al. (1988) LVG solutions are taken from the upper right region of Fig. 2, where emission begins to dominate absorption. Solutions with $X(C_3H_2)/(dv/dr) \lesssim 10^{-7}$ km^{-1} s pc were found in this region for the current observations, but rejected because a small increase in density would result in emission instead of absorption. For a sample of several clouds, some emission lines would be expected if these high abundances were really present, but no emission was seen, implying that the low abundance solutions are the correct ones. The production of C_3H_2 does not, therefore, need to be as rapid in diffuse clouds as was previously supposed (Cox et al. 1988).

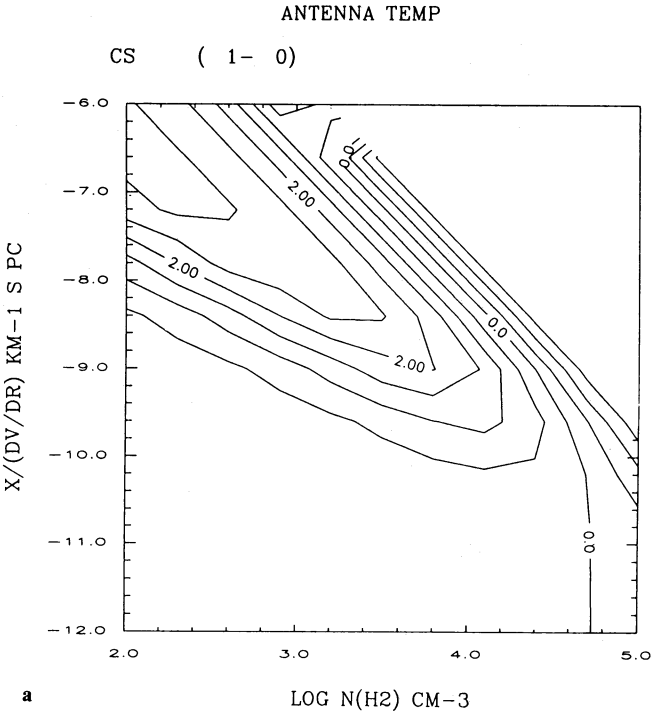

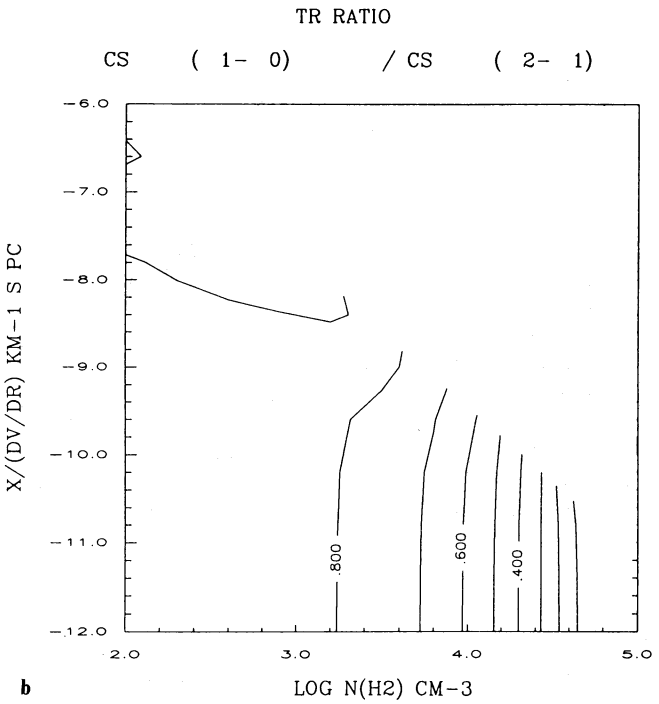

Fig. 2a and b. LVG model output plots, for $T_{kin}=10$ K. The axes are abundance relative to H_2, divided by velocity gradient, against H_2 density. **a** CS $J=1$–0 T_R contours. Positive values indicate absorption against the continuum, and negative values emission. Strong emission occurs in the upper right corner of the plot, where the contours are too closely spaced to be shown. The contour interval is 0.5 K. **b** Contours of the ratio T_R (CS $J=1$–0)/T_R (CS $J=2$–1). The values in the upper right corner of the plot are uncertain, where there is a rapid transition from absorption to emission, and these have been omitted. The contour interval is 0.1

Table 5. Results from LVG analysis. All quantities are for the position Sgr B2 "M", as insufficient CS absorption data was obtained to estimate densities for other positions. The assumed value of T_{kin} was 10 K. Logs are to base 10. Errors from the uncertainties in the line strengths are $\pm$ (0.2–0.5) on log n_{H_2} and log $X/(dv/dr)$, and the corresponding errors on τ and T_{ex} are factors $\lesssim 3$ and $\lesssim {}^{+3}_{-1}$ K, respectively; hence the optical depths and excitation temperatures are not well determined

v_{lsr} (km s^{-1})	Transition	log n_{H_2} (cm^{-3})	log $X/(dv/dr)$ (km^{-1} s pc)	τ	T_{ex} (K)
+ 3	CS $J = 1$–0	3.7	− 9.4	0.6	3.1
	CS $J = 2$–1		− 9.4	0.8	2.9
	$H^{13}CN$ $J = 1$–0		− 10.2	0.6	2.7
	$H^{13}CO^+$ $J = 1$–0		− 10.9	0.2	2.8
	C_3H_2 $2_{1,2}$–$1_{0,1}$		− 10.3	0.2	2.8
− 25	CS $J = 1$–0	4.0	− 10.2	0.2	3.4
	CS $J = 2$–1		− 10.2	0.3	2.9
	C_3H_2 $2_{1,2}$–$1_{0,1}$		− 10.8	0.1	2.9
− 42	CS $J = 1$–0	3.6	− 9.2	0.8	3.0
	CS $J = 2$–1		− 9.2	1.1	2.9
	$H^{13}CN$ $J = 1$–0		− 10.5	0.2	2.7
	$H^{13}CO^+$ $J = 1$–0		− 10.8	0.3	2.8
	C_3H_2 $2_{1,2}$–$1_{0,1}$		− 10.2	0.2	2.7
− 46	CS $J = 1$–0	4.3	− 10.2	0.3	4.1
	CS $J = 2$–1		− 10.2	0.5	3.2
	C_3H_2 $2_{1,2}$–$1_{0,1}$		− 11.0	0.2	3.0
− 73	CS $J = 1$–0	4.2	− 10.3	0.2	3.7
	CS $J = 2$–1		− 10.3	0.3	3.1
	C_3H_2 $2_{1,2}$–$1_{0,1}$		− 10.9	0.2	3.0
− 105	CS $J = 1$–0	4.0	− 9.7	0.5	3.5
	CS $J = 2$–1		− 9.7	0.9	3.0
	H^{13} CN $J = 1$–0		− 11.0	0.2	2.8
	$H^{13}CO^+$ $J = 1$–0		− 11.3	0.2	3.0
	C_3H_2 $2_{1,2}$–$1_{0,1}$		− 10.7	0.2	3.0

For $T_{kin} > 10$ K, the n_{H_2} solutions are decreased, and the corresponding values of $X/(dv/dr)$ increased. (The T_{ex} value found is almost independent of T_{kin}.) For T_{kin} as high as 50 K, the abundance estimate is approximately a factor of 3 greater than for $T_{kin} = 10$ K, and the density is a factor of 3 lower. If the true cloud densities are not $\sim 10^4$ cm^{-3}, but only $\sim 10^3$ cm^{-3}, as was previously believed, the kinetic temperatures of the gas must be high (> 50 K). In this case, the molecular gas would be at a similar temperature to the atomic (H I) component in diffuse clouds, for which $T_{kin} \sim 50$–100 K (Bell et al. 1981; Davies & Matthews 1972).

4. Discussion

Absorption lines from 7 diffuse clouds have been observed, in isotopic variants of 5 molecular species. All of these molecules are small, with 5 or less atoms, and larger species detected in emission in the Sgr B2 spectral survey (e.g. HC_5N) were not found in absorption in the foreground clouds. This does not necessarily imply a simple chemistry in diffuse clouds, since the line strengths from large species are expected to be small. At 42–98 GHz, their transitions will have high J values and, for low T_{ex}, small level populations. For example, towards Sgr B2, a molecule with a rotational constant a factor of 5 smaller than that of CS will have absorption lines a factor ~ 50 weaker at ~ 100 GHz.

The absorption features detected are mostly optically thin, with molecular column densities $N \sim 10^{12-14}$ cm^{-2} per diffuse cloud. (These low column densities were easily detectable, because the low T_{ex} ensures that most of the molecules are in the low-J levels giving strong $J = 1$–0 and 2–1 transitions.) The relative abundances of the various species were similar in all the clouds. This result contrasts with the conclusions of Miyawaki et al. (1988), who compared the abundances of various species detected in absorption towards W49A. For gas at $v_{lsr} \approx 39$ km s^{-1}, CS was found to be more abundant by factors ~ 5, when compared to other species, than in material at $v_{lsr} \approx 60$ km s^{-1}. This result is inconclusive, however, since some of the transitions used for comparison are likely to be optically thick. For example, the continuum is almost wholly absorbed in HCO^+ $J = 1$–0 at $v_{lsr} \approx 39$ and 60 km s^{-1}, implying $\tau \gg 1$. The column densities of HCO^+ are, therefore, only known to within an order of magnitude (Nyman 1983).

SiO absorption in diffuse clouds has been observed for the first time, at 2 different velocities. (These data have also been discussed by Ohishi 1991). The abundance of SiO is unexpectedly high, with column densities comparable to CS. This species has previously only been detected (in emission) in compact regions of warm gas, and was thought to be produced only in hot and/or shocked zones (Ziurys et al. 1989; Ziurys & Friberg 1987). The detection of SiO in diffuse gas with low excitation temperatures suggests that the theory of SiO production needs to be revised.

Further observations are needed to determine the types of diffuse cloud in which this species has a high abundance. The present data show that it is located in the gas in spiral arms ($v_{lsr}=+3$ km s^{-1}) and Galactic Centre ($v_{lsr}=-105$ km s^{-1}), but not in the 3 kpc expanding arm ($v_{lsr}=-42$ and -46 km s^{-1}).

4.1. Identification of clouds

Most of the absorption features described in this paper were detected in 5 GHz H_2CO absorption by Whiteoak & Gardner (1979). The lines at $+67$, $+3$, -44, and <-50 km s^{-1} are associated by these authors with, respectively, a cloud physically associated with the Sgr B2 cores; gas within a few hundred parsecs of the Sun; the expanding arm at ~ 3 kpc from the Galactic Centre; and the "nuclear disk" (radius ~ 1 kpc) which lies at the centre of the Galaxy. The $+3$ km s^{-1} gas probably also includes absorption in the Sagittarius and Scutum arms at galactocentric distances of 5–8 kpc (see Bally 1987). Additional features at $v_{lsr}=+30$ and -25 km s^{-1} have yet to be identified.

The $+30$ km s^{-1} gas is interesting because ^{13}CO $J=1$–0 maps by Bally et al. (1988) show a ring of gas at this velocity, around a hole where little emission is seen in the Sgr B2 direction. They concluded that it was unlikely that ^{13}CO emission was absorbed by cold gas, and hence that there was a genuine absence of material. The present observations show that there *is* absorbing gas at this velocity.

The absorption at -25 km s^{-1} may arise from a feature attributed by Whiteoak & Gardner (1979) to a cloud at ~ 4.5 kpc from the Galactic Centre. The double structure of this line suggests it may be due to an arm, similar to the 3 kpc expanding arm (double spectrum at -42 and -46 km s^{-1}). The line splitting could result from material ahead of and behind the arm having lower density than the arm itself. Denser gas will be more highly excited; therefore, absorption will be weaker, as shown by the LVG modelling. Consequently, two absorption minima are seen, at different velocities.

The lines at <-50 km s^{-1} relate to the "nuclear disk". This very extended feature (radius ~ 1 kpc) is dominated by non-circular motions, and is tilted out of the Galactic Plane. Estimates of the degree of tilt range from 5–30° (Sanders et al. 1984; Güsten & Downes 1980). Mapping of 2.4 μm emission by Matsumoto et al. (1982) has been interpreted by Blitz & Spergel (1991) to show that the material within ~ 1 kpc forms a bar. Previous absorption line observations towards Sgr B2 (Linke et al. 1981) were consistent with models of gas orbits distributed throughout such a bar (Liszt & Burton 1980), showing nearly complete absorption of the continuum by HCN and HCO^+ $J=1$–0 in the velocity range -129 to $+2$ km s^{-1}. This result is misleading, since these lines are optically thick ($\tau\sim 3$, based on the results of Table 4 for the ^{13}C-isotopomers and $[^{12}C/^{13}C]\approx 30$ near the Galactic Centre, Wannier 1989). The current data show that the absorption profiles are not flat-bottomed, as in the Linke et al. (1981) spectra, but have at least two distinct dips, at -73 and -105 km s^{-1}. These profiles do *not* fit the models of a homogeneous bar, but the -105 km s^{-1} absorption is consistent with the restricted-orbits model by Binney et al. (1991). It, therefore, appears that the dips observed in the current spectra may arise from gas following particular paths in a bar around the Galactic Centre, while the widespread CO emission (Liszt & Burton 1978) traces less dense material following many different trajectories.

5. Conclusions

The NRO 45 m and JCMT 15 m telescopes have been used to observe towards Sgr B2 at frequencies of 42, 49, 85, 98, 230 and 330–360 GHz. Absorption lines from 7 diffuse clouds at different velocities were detected, against the Sgr B2 continuum emission. These clouds are located in the "nuclear disk", 3 kpc expanding arm, spiral arms in the Galactic Plane, and (tentatively) ~ 4.5 kpc from the Galactic Centre. Species detected in absorption include CS, C_3H_2, HCN, HCO^+ and SiO. The detection of SiO in cool diffuse gas suggests that the theories of its production only in hot and/or shocked regions need to be revised. Evidence was found for a $[^{32}S:{}^{34}S]$ isotopic ratio of ~ 6–15 in the diffuse clouds, a factor ~ 2 less than in dark clouds.

The absorption lines are mostly optically thin, with column densities of 10^{12-14} cm^{-2} per cloud. Excitation temperatures of up to 5 K were found, implying more heating than can be supplied by the 2.7 K cosmic background radiation. The clouds are chemically uniform in most species, and LVG modelling results suggest an average cloud H_2 density of 10^4 cm^{-3}.

Features at $v_{lsr}\approx -73$ and -105 km s^{-1} can be attributed to gas within ~ 1 kpc of the Galactic Centre. The profiles observed are *not* consistent with the previous models of a homogeneous disk or bar, instead suggesting that the diffuse clouds lie on constrained orbits.

Acknowledgements. We thank the staff at the NRO and JCMT for their support at the telescopes, and the UK Science and Engineering Research Council for travel funding, the support of millimetre and sub-millimetre astronomy at QMW, and a fellowship for JSG. The JCMT is operated by the Royal Observatory, Edinburgh, on behalf of the SERC, the Netherlands Organisation for Pure Research and the National Research Council of Canada. GJW thanks the NRO for a stimulating and productive subbatical in Japan. JSG expresses her gratitude to C.A. Sanderson for many useful and lively discussions of the data.

Appendix A: LTE equations for absorption lines

For absorption against the continuum alone (no background molecular emission), the total antenna temperature seen is

$$T_R(c+l)=(1-e^{-\tau})b(T_{ex})+e^{-\tau}[b(T_{cont})+b(2.7)]-b(2.7), \quad (A1)$$

where τ and T_{ex} are the optical depth and excitation temperature of the absorbing gas, T_{cont} is the blackbody continuum temperature, $b(T)$ is the emission function $(h\nu/k)(e^{h\nu/kT}-1)^{-1}$, and $b(2.7)$ is the contribution from the 2.7 K cosmic background radiation. The last term in Eq. (A1) is the cosmic background emission subtracted out by position switching.

The antenna temperature of the absorption line is defined as $T_R(c+l)-T_R(c)$, where the continuum strength $T_R(c)$ is given by $b(T_{cont})$, since the 2.7 K contribution is again removed by position switching. The line strength is, therefore,

$$T_R(l)=(1-e^{-\tau})[b(T_{ex})-b(T_{cont})-b(2.7)], \quad (A2)$$

where $T_R(l)<0$. From Eq. (A2), the optical depth is given by

$$\tau\geq -\ln[1+T_R(l)/T_R(c)] \quad (A3)$$

and the lower limit applies if $T_{ex}=2.7$ K. (The excitation temperature cannot be less than 2.7 K, since the cosmic background radiation will excite the molecules until temperature equilibrium is reached.) The value of τ varies considerably for a small range of

T_{ex} values. Previous authors have often assumed an excitation temperature of 2.7 K, but this can result in τ being underestimated by an order of magnitude.

Similar equations can be derived for profiles combining background emission and absorption, but for the Sgr B2 observations the optical depths obtained have large errors (factors ≥ 2). This is because the asymmetry of the lines results in considerable uncertainty in the estimates of background emission intensity. Consequently, these results have not been included here.

The integrated intensity of an absorption transition is related to the column density of molecules via

$$\int I_\nu \, d\nu = -(h\nu/4\pi)(B_{lu}\rho_\nu N_l - A_{ul}N_u - B_{ul}\rho_\nu N_u), \quad \text{(A4)}$$

where I_ν is the intensity at frequency ν, N_l and N_u are the number of molecules per unit area in the lower (l) and upper (u) levels of the transition, B_{lu}, B_{ul} and A_{ul} are the Einstein coefficients for absorption and stimulated and spontaneous emission, and ρ_ν is the radiation field energy density. Substituting standard expressions for the Einstein coefficients and radiation density, and using the Boltzmann equation to relate N_u and N_l gives

$$\int T_R(l)\, d\nu = -\frac{\kappa\nu^2 S e^{-E_l/kT_{ex}}}{Z(T_{ex})} \frac{1-e^{(h\nu/k)(1/T_{cont}-1/T_{ex})}}{e^{h\nu/kT_{cont}}-1} N \quad \text{(A5)}$$

(for optically thin lines), where $\kappa = 8\pi^3\mu^2/3kc$, μ is the permanent electric dipole moment of the molecule, S is the transition strength (J_u for linear species), E_l is the energy of the lower level above the $J=0$ state, $Z(T_{ex})$ is the partition function, and N is the column density summed over all levels. Equation (A5) shows that absorption is only observed when $T_{ex} < T_{cont}$. This is intuitively correct, since the background radiation will be hotter than the cloud and, hence, will be absorbed to bring the radiation and gas towards temperature equilibrium.

The excitation temperature can be estimated by taking the ratio of the integrated antenna temperatures in Eq. (A5), for two different transitions of the same species. For adjacent transitions of a linear species, denoted by 1 ($J \rightarrow J-1$) and 2 ($J+1 \rightarrow J$), this gives

$$\frac{\int T_R(1)\, d\nu}{\int T_R(2)\, d\nu} = \frac{\nu_1}{\nu_2}\frac{J}{J+1}\frac{e^{h\nu_1/kT_{ex}}-1}{1-e^{-h\nu_2/kT_{ex}}}\frac{T_{cont}(1)}{T_{cont}(2)}, \quad \text{(A6)}$$

from which T_{ex} can be found. It is assumed in the derivation of Eq. (A6) that $h\nu \ll kT_{cont}$, and that $T_{cont} \gg T_{ex}$. This is certainly the case for the Sgr B2 observations, where $T_{cont} \sim 35$ K (Goldsmith et al. 1987) and $T_{ex} \approx 3$–5 K. Note that the expressions for T_{ex} and N are not affected by beam-dilution (for filling factor $\eta_c \ll 1$ and $T_{cont} \gg T_{ex}$), since the η_c terms for the line and continuum cancel out.

References

Akabane K., Sofue Y., Hirabayashi H., Morimoto M., Inoue M., 1988, PASJ 40, 459

Bally J., 1987, in: Reipurth B. (ed.) Proceedings of the ESO Workshop on Low-Mass Star-Formation and Pre-main Sequence Objects. European Southern Observatory, Garching, p. 1

Bally J., Stark A.A., Wilson R.W., Henkel C., 1987, ApJS 65, 13

Bally J., Stark A.A., Wilson R.W., Henkel C., 1988, ApJ 324, 223

Bell M.B., Feldman P.A., Matthews H.E., 1981, A&A 101, L13

Binney J., Gerhard O.E., Stark A.A., Bally J., Uchida K.I., 1991, MNRAS 252, 210

Blake G.A., Sutton E.C., Masson C.R., Phillips T.G., 1987, ApJ 315, 621

Blitz L., Spergel D.N., 1991, ApJ 379, 631

Cox P., Güsten R., Henkel C., 1988, A&A 206, 108

Davies R.D., Matthews H.E., 1972, MNRAS 156, 253

Downes D., Wilson T.L., Bieging J., Wink J., 1980, A&AS 40, 379

Goldsmith P.F., Snell R.L., Lis D.C., 1987, ApJ 313, L5

Goldsmith P.F., Lis D.C., Hills R., Lasenby J., 1990, ApJ 350, 186

Gordon M.A., Jewell P.R., Kaftan-Kassim M.A., Salter C.J., 1986, ApJ 308, 288

Greaves J.S., 1990, Ph.D. Thesis, University of London

Greaves J.S., Williams P.G. (in preparation)

Güsten R., Downes D., 1980, A&A 87, 6

Hartquist T.W., Oppenheimer M., Dalgarno A., 1980, ApJ 236, 182

Hollenbach D., 1988, Astron. Lett. Communication 26, 191

Irvine W.M., Goldsmith P.F., Hjalmarson Å., 1987, in: Hollenbach D.J., Thronson H.A. Jr. (eds.) Proceedings of the Symposium on Interstellar Processes. Reidel, Dordrecht, p.561

Kogut A., Smooth G.F., Bennett C.L., Petuchowski S.J., 1989, ApJ 346, 763

Linke R.A., Stark A.A., Frerking M.A., 1981, ApJ 243, 147

Lis D.C., Goldsmith P.F., 1990, ApJ 356, 195

Lis D.C., Goldsmith P.F., 1991, ApJ 369, 157

Liszt H.S., Burton W.B., 1978, ApJ 226, 790

Liszt H.S., Burton W.B., 1980, ApJ 236, 779

Matsumoto T., Hayakawa S., Koizumi H., et al., 1982, in: Reigler G., Blandford R. (eds.) The Galactic Center. American Institute of Physics, New York, p. 48

Matthews H.E., Irvine W.M., 1985, ApJ 298, L61

Miyawaki R., Hasegawa T., Hayashi M., 1988, PASJ 40, 69

Nyman L.-Å., 1983, A&A 120, 307

Nyman L.-Å., 1984, A&A 141, 323

Nyman L.-Å., Millar T.J., 1989, A&A 222, 231

Ohishi M., 1991, in: Kaifu N. (ed.) Chemistry and Spectroscopy of Interstellar Molecules. University of Tokyo Press, Tokyo

Sanders D.B., Solomon P.M., Scoville N.Z., 1984, ApJ 276, 182

Tosi M., 1982, ApJ 254, 699

Wannier P.G., 1980, ARA&A 18, 399

Wannier P.G., 1989, in: Morris M. (ed.) Proc. IAU Symp. 136, The Centre of the Galaxy. Kluwer, Dordrecht, p. 107

White G.J., Ohishi M., Hasegawa T., et al. (in preparation)

Whiteoak J.B., Gardner F.F., 1979, MNRAS 188, 445

Ziurys L.M., Friberg P., 1987, ApJ 314, L49

Ziurys L.M., Friberg P., Irvine W.M., 1989, ApJ 343, 201